



# Acoustic modelling of the installation effects of a subsonic jet beneath a flat plate

Étienne Spieser\* and Christophe Bailly†

*Univ Lyon, École Centrale de Lyon, CNRS, Univ Claude Bernard Lyon 1, INSA Lyon, LMFA, UMR5509, 69130, Écully, France*

César Legendre‡

*Free Field Technologies (part of Hexagon's Manufacturing Intelligence division), Axis Park Louvain-la-Neuve, 9 rue Émile Francqui, B-1435 Mont-Saint-Guibert, Belgium*

**Tam and Auriault's statistical mixing noise model has been reformulated by the authors so to be able to compute propagation effects with help of Pierce's wave equation, that is fairly accurate and acoustic preserving. This study presents predictions computed with this model for the sound emitted by two Mach 0.9 round jets. One is isolated, the other one is installed beneath a flat plate. Tailored adjoint Green's functions are computed using the finite element solver Actran <sup>TM</sup>. The methodology is able to retrieve acoustic measurements within 2 dB for a range of Strouhal numbers of more than two orders of magnitude. For an observer located close to the jet axis, at polar angle  $\theta$  smaller than  $\theta = 50^\circ$ , poorer predictions are obtained however. It is found that Tam and Auriault's mixing noise model designed for the radiation of the turbulence fine scales does not radiate isotropically but peaks instead around  $\theta = 45^\circ$ . Tailored adjoint Green's functions computed for the isolated and installed configuration demonstrate the ability of the proposed methodology to account for propagation effects due to the flow and the presence of surfaces.**

## I. Introduction

Since the early assessment by Lighthill, seventy years ago [1], of the acoustic intensity radiated by a turbulent flow, a number of improvements have been made in the modelling of the sound emitted by jets. Acoustic spectra are now commonly inferred from a RANS solution of the jet flow, and involve the subtle combination of many ingredients. Among these are the choice of an acoustic analogy such as Lighthill's [2], Lilley's [3], LEE [4], GAA [5], or based on Pierce's equation [6]; the calibration [7] [8] and the modelling of the sound source intercorrelation with for instance a Gaussian function [9] [10], an exponential function [7] or a hyperbolic cosine function [11]. The choice of a fixed [5] or moving [7] reference frame for the source modelling; the account of the source convection [1] [12]; the taking into account of the source compactness [13] as well as the choice of a turbulence model for the source [14] [3] [15] [16] are other parameters to be set. Various approximations to simplify the double integral applying on the source volume can be made, such as a Fraunhofer-like approximation [10] or a Taylor expansion [6]. The calculation of the sound propagation can then be computed directly [17] [18], or addressed with an adjoint approach that takes benefit from the reciprocity principle to recast the radiation problem [19] [20] [21]. Green's functions can then be solved analytically or numerically as well for the direct problem [22] [23] as for the adjoint one [24] [6].

In the present work, a recast of Tam and Auriault's mixing noise model for the acoustic potential [25] is retained. As for their original contribution [10], an isotropic Gaussian model for the sound source intercorrelation set in a moving reference frame is considered. In the same way, the double volume integral is simplified assuming that Fraunhofer's condition is fulfilled. Sound propagation is consistently solved within the adjoint framework. Compared to the original model, the propagation of sound is modelled with Pierce's wave equation which represents an elegant alternative to the full set of LEE for being scalar, acoustic preserving and fairly accurate. Adjoint Green's functions to Pierce's wave equation are solved by means of the flow reversal theorem (FRT), which proved to be equivalent to the adjoint approach for self-adjoint operators [21]. The authors have shown how the finite element solver Actran <sup>TM</sup> could be

\*Postdoctoral Fellow, Fluid Mechanics and Acoustics Laboratory (LMFA).

†Professor, Fluid Mechanics and Acoustics Laboratory (LMFA), AIAA Senior member.

‡Aeroacoustic Development Leader & Senior Research Engineer.

used to compute such adjoint Green's functions for an isolated jet for an observer normal to the flow direction [6]. This procedure is used in the following. This represents the major change with respect to the reference model [10], and the focus is therefore laid on the ability of this formulation to properly account for propagation effects in an installed configuration and for angles that are not normal to the jet axis. The installation effects on the acoustic radiation of a jet beneath a flat plate are investigated. Predictions obtained with the model are compared with measurements carried out at the Pprime laboratory [26]. The present contribution aims to demonstrate that the presence of flow and surfaces can be dealt in the computation of adjoint Green's functions. In the first part of this paper, the jet noise model considered is briefly recalled. Then, to verify the model's accuracy at angles shallow to the jet axis, predictions obtained in the downstream direction of an isolated round jet are compared with measurements. In a last section, acoustic spectra radiated by the installed jet in the nozzle exhaust plan are computed and compared to measurements for various azimuthal angles.

## II. Tam and Auriault's mixing noise model reformulated for Pierce's wave equation

### A. Governing equations

In their study [10], Tam and Auriault have shown that the source of flow noise associated with turbulent mixing could be described with some success considering solely the fluid dilatation and compression. This standpoint, inspired from the kinetic theory of gases, entails following simplification of the Reynolds stress tensor,

$$\rho_0 \mathbf{u}' \otimes \mathbf{u}' \approx q_s \mathbf{I}_d \quad (1)$$

where  $q_s$  measures the compression caused by the fluid fluctuations,  $\mathbf{I}_d$  is the identity matrix,  $\rho_0$  is the fluid mean density and  $\mathbf{u}'$  corresponds to the fluctuating velocity. Acoustic fluctuations generated by the turbulent mixing process of a jet is then described by,

$$\begin{cases} \rho_0 \frac{D\mathbf{u}'}{Dt} + \nabla p' = -\nabla q_s \\ \frac{Dp'}{Dt} + \gamma p_0 \nabla \cdot \mathbf{u}' = 0 \end{cases} \quad (2)$$

where  $D/Dt = \partial/\partial t + \mathbf{u}_0 \cdot \nabla$  is the material derivative along the mean flow,  $p_0$  and  $p'$  are the pressure mean value and fluctuations respectively, and  $\gamma$  corresponds to the adiabatic index of air. Assuming the acoustic fluctuations can be described by an acoustic potential  $\phi$  given by  $\nabla \phi = \rho_0 \mathbf{u}'$  and  $p' = -D\phi/Dt$ . Tam and Auriault's mixing noise model can be recast with Pierce's wave equation into,

$$\frac{D^2 \phi}{Dt^2} - \nabla \cdot (a_0^2 \nabla \phi) = -\frac{D q_s}{Dt}, \quad (3)$$

### B. Adjoint statement of the problem

In statistical jet noise modelling, it is convenient to separate noise generation mechanism from the sound propagation in choosing an adjoint framework [20] [10] [25]. This is done here by considering adjoint Green's functions  $\phi_{\mathbf{x}_m, t_m}^\dagger$  associated with Pierce's wave equation for the canonical scalar product and for an observer located at  $\mathbf{x}_m$  and a listening time  $t_m$ ,

$$\frac{D^2 \phi_{\mathbf{x}_m, t_m}^\dagger}{Dt^2} - \nabla \cdot (a_0^2 \nabla \phi_{\mathbf{x}_m, t_m}^\dagger) = \delta(\mathbf{x}_m - \mathbf{x}) \delta(t_m - t) \quad (4)$$

where the anti-causal solution of previous equation has to be computed. Equation (4) is solved using FRT [21]. The physical meaningful acoustic fluctuations are then recovered from Lagrange's identity [21],

$$\phi(\mathbf{x}_m, t_m) = - \langle \phi_{\mathbf{x}_m, t_m}^\dagger, \frac{Dq_s}{Dt} \rangle \quad (5)$$

### C. Modelling of the acoustic noise spectra

Previous expression for the acoustic potential  $\phi$  is used to compute the acoustic power spectral density,

$$S_{pp}(\mathbf{x}_m, \omega) = \lim_{T \rightarrow \infty} \frac{1}{T} \int_{\mathbb{R}} d\tau \int_{-T/2}^{T/2} dt_m \frac{D\phi}{D_{t_m, \mathbf{x}_m}} \frac{D\phi}{D_{t_m + \tau, \mathbf{x}_m}} e^{i\omega\tau} \quad (6)$$

where  $D/D_{t_i, \mathbf{x}_j}$  is the material derivative expressed for a time  $t_i$  and position  $\mathbf{x}_j$ , and  $\omega$  is the angular frequency of the sound. In Tam and Auriault's mixing noise model, the sound source intercorrelation reads [10] [25],

$$\lim_{T \rightarrow \infty} \frac{1}{T} \int_{-T/2}^{T/2} \frac{D q_s}{D_{t_s, \mathbf{x}_1}} \frac{D q_s}{D_{t_s + \tau, \mathbf{x}_2}} = \frac{\hat{q}_s^2}{c^2 \tau_s^2} \exp \left( -\frac{|\mathbf{r} \cdot \mathbf{u}_0|}{u_0^2 \tau_s} - \frac{\ln(2)}{l_s^2} (r - \tau \mathbf{u}_0)^2 \right) \quad (7)$$

where  $l_s$  and  $\tau_s$  are respectively the characteristic length and time of the turbulence intercorrelation, and  $\hat{q}_s/c$  is the strength of the modelled source of sound. After some derivations detailed in [25],

$$S_{pp}(\mathbf{x}_m, \omega) = \int_{\Omega} d\mathbf{x}_2 \frac{2\hat{q}_s^2 l_s^3}{c^2 \tau_s} \left( \frac{\pi}{\ln(2)} \right)^{3/2} \left| D_{-\mathbf{u}_0, \mathbf{x}_m} \left( \phi_{\mathbf{x}_m}^{\dagger}(\mathbf{x}_2, \omega) \right) \right|^2 \frac{\exp \left( \frac{-\omega^2 l_s^2}{4 \ln(2) u_0^2} \left( 1 + \frac{u_0^2 |\mathbf{x}_{m, \perp}|^2}{a_{\infty}^2 |\mathbf{x}_m|^2} \right) \right)}{1 + \omega^2 \tau_s^2 \left( 1 - \frac{\mathbf{u}_0 \cdot \mathbf{x}_m}{a_{\infty} |\mathbf{x}_m|} \right)^2} \quad (8)$$

where  $a_{\infty}$  is the ambient speed of sound, and  $\mathbf{x}_{m, \perp} = \mathbf{x}_m - (\mathbf{x}_m \cdot \mathbf{u}_0) \mathbf{u}_0 / u_0^2$ . The material derivative  $D_{-\mathbf{u}_0, \mathbf{x}_m} \left( \phi_{\mathbf{x}_m}^{\dagger}(\mathbf{x}_2, \omega) \right)$  can be expressed analytically in presence of flight effects, that is when the ambient media is moving at a constant Mach number  $M_f$ . In the end, for a microphone located in the far-field at a polar angle  $\theta_m$  from the jet axis, Tam and Auriault's mixing noise formula can be recast for Pierce's wave equation into,

$$S_{pp}(\theta_m, \omega) = \int_{\Omega} d\mathbf{x}_2 \ 2 \left( \frac{\pi}{\ln(2)} \right)^{3/2} \frac{\omega^2 \hat{q}_s^2 l_s^3}{c^2 \tau_s} C_f \left| \phi_{\theta_m}^{\dagger}(\mathbf{x}_2, \omega) \right|^2 \frac{\exp \left( \frac{-\omega^2 l_s^2}{4 \ln(2) u_0^2} (1 + M_{\infty}^2 \sin^2 \theta_m) \right)}{1 + \omega^2 \tau_s^2 (1 - M_{\infty} \cos \theta_m)^2} \quad (9)$$

Where azimuthal dependences on the observer location are discarded in the formula, for simplicity and because the jets investigated here are round. Note that it is straightforward to include these dependences in the model from equation (8). And where  $C_f$  corresponds to the analytically computed flight effects,

$$C_f = \left( 1 + \frac{M_f \cos \theta_m}{1 + M_f \cos \theta_m} \right)^2 \quad (10)$$

#### D. Calibration of the constants appearing in the model

The time  $\tau_s$  and length  $l_s$  of reference are connected here to each other by a characteristic velocity  $u'_{\text{ref}}$  such that,

$$l_s = u'_{\text{ref}} \tau_s \quad \text{with} \quad u'_{\text{ref}} = \sqrt{\frac{2}{3} k_{\text{max}}} \quad (11)$$

From dimensional considerations the characteristic length  $l_s$  can be rebuilt from  $k$ , the turbulent kinetic energy in [ $\text{m}^2 \cdot \text{s}^{-2}$ ], and  $|\partial u_z / \partial r|_{\text{max}}$ , the maximal shear in each axial section of constant  $z$  in [ $\text{s}^{-1}$ ] considering,

$$l_s \propto \sqrt{k} / \left| \frac{\partial u_z}{\partial r} \right|_{\text{max}} \quad (12)$$

The parameter  $\hat{q}_s/c$  that corresponds to the amplitude of the sound source is simply modelled in accordance with equation (1) as,

$$\frac{\hat{q}_s}{c} \propto \rho_0 k \quad (13)$$

Compared to the original model of Tam and Auriault [10], these parameters do not require the computation of the turbulent dissipation rate  $\varepsilon$ , and thus RANS solvers based on different turbulence models can be used. This work uses the statistics of the jet flow computed with a RANS solver relying on a ( $k$ - $\omega$ ) closure model to inform the set of parameters appearing in Tam and Auriault's source model. The constants  $k_{\text{max}}$  and  $|\partial u_z / \partial r|_{\text{max}}$  computed for each axial positions of the Mach 0.9 round jet investigated in this work are presented in figure 1. The evolution along the jet axis of the constants  $k_{\text{max}}$  and  $|\partial u_z / \partial r|_{\text{max}}$  is smooth and it would be fairly easy to replace these curves with a fitting semi-empirical model.

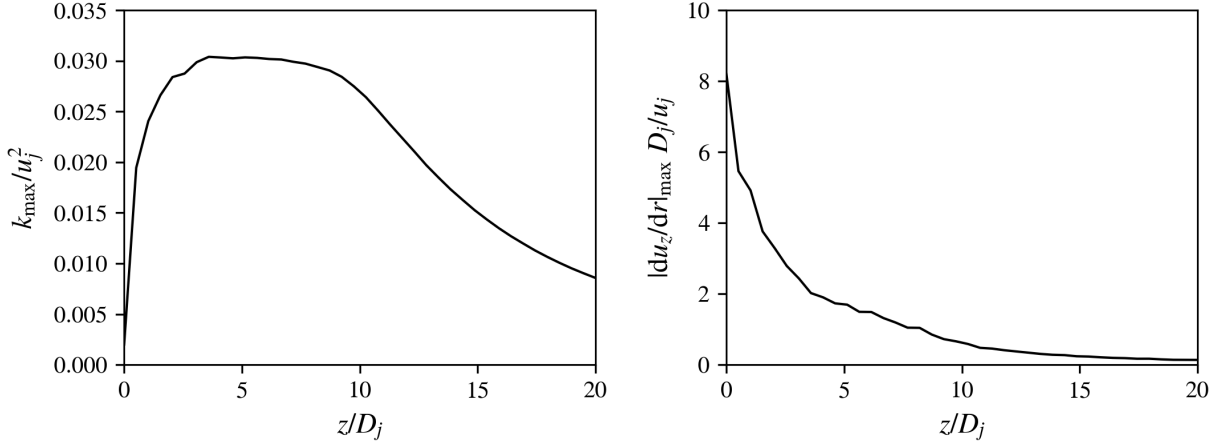


**Fig. 1** Evolution of the normalised maximal turbulent kinetic energy  $k_{\max}$ , and of the normalised maximal shearing of the jet flow  $|\partial u_z/\partial r|_{\max}$ .

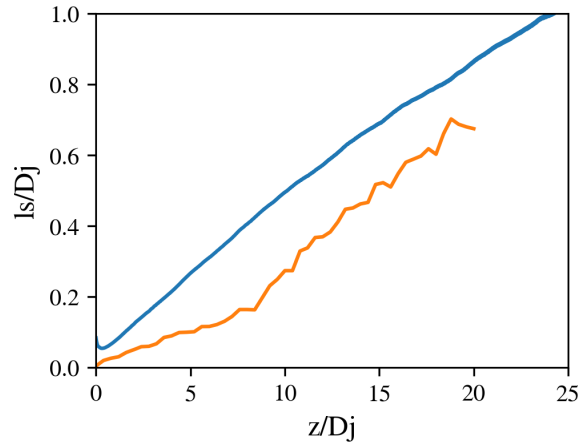


**Fig. 2** Evolution of the characteristic length  $l_s$  along the jet lipline. —, reference computed from the integral length scale of a LES [25], and, —, characteristic length  $l_s$  computed from equation (12) with a proportionality constant of 1.0.

The characteristic length  $l_s$  of Tam and Auriault’s model is calibrated with the integral length scale computed along the jet lipline of a LES computation as done in [25]. Figure 2 presents the evolution of  $l_s$  along the jet lipline as computed with equation (12) and compared to a reference solution. The characteristic length  $l_s$  computed from equation (12) displays a broken line composed by two lines that intersect at the closure location of the jet potential core. The growth of  $l_s$  is more rapid in the fully developed jet region than in the potential core zone. The characteristic length  $l_s$  presented in figure 2 is computed from equation (12) with a proportionality constant of 1.0. In the developed region, that is for  $z \gtrsim 8D_j$  the slope of the computed characteristic length matches with the reference solution inferred from the LES solution. The characteristic time scale  $\tau_s$  of Tam and Auriault’s mixing noise model is rebuilt subsequently using equation (11).

To calibrate the amplitude  $\hat{q}_s/c$  of the source autocorrelation as computed with equation (13), the noise spectra measured at  $\theta_m = 90^\circ$  in the far field of a round jet is taken as reference. The measurements carried out at Pprime on a Mach 0.9 isolated round jet, and presented in next section, are considered. The noise spectra are expressed in  $dB/St$ , they are normalised to a distance of 1 m and compensated so as to correspond to an equivalent jet of section  $1 \text{ m}^2$ . The Fourier transform of the pressure autocorrelation  $S_{pp}$  obtained with Tam and Auriault’s formula is hence related to

this normalised sound power level (SPL) by,

$$SPL(dB/St) = 10 \log_{10} \left( \frac{S_{pp}(\mathbf{x}_m, \omega)}{p_{\text{ref}}^2} \right) + 10 \log_{10} \left( \frac{u_j}{D_j} \right) - 10 \log_{10} \left( \frac{\pi D_j^2}{4} \right) + 10 \log_{10} (|\mathbf{x}_m|^2) \quad (14)$$

where  $p_{\text{ref}} = 20.0 \mu\text{Pa}$  and  $|\mathbf{x}_m|$  corresponds to the distance from the jet exhaust to the microphone position. The Strouhal number  $St$  is based on the jet diameter  $D_j$  and exhaust velocity  $u_j$  such that,  $St = \omega D_j / (2\pi u_j)$ . At  $\theta_m = 90^\circ$  from the jet axis, mean flow refraction effects are deemed not of leading order and without external wind, Green's function appearing in Tam and Auriault's formula may be approximated with [25],

$$\left| \phi_{\mathbf{x}_m}^*(\mathbf{x}, \omega) \right|^2 = \frac{1}{16\pi^2 a_0^4 |\mathbf{x} - \mathbf{x}_m|^2}. \quad (15)$$

This analytical Green's function is injected in equation (9) and serves to calibrate the amplitude. Figure 3 compares acoustic measurements at  $\theta_m = 90^\circ$  from a  $M_j = 0.9$  round jet [27] with the corresponding predictions obtained when a unitary proportionality constant is used for equation (13). The values of  $l_s$  and  $\tau_s$  calibrated as earlier are considered. The fit between predictions and measurements is remarkable in amplitude, shape and central frequency.

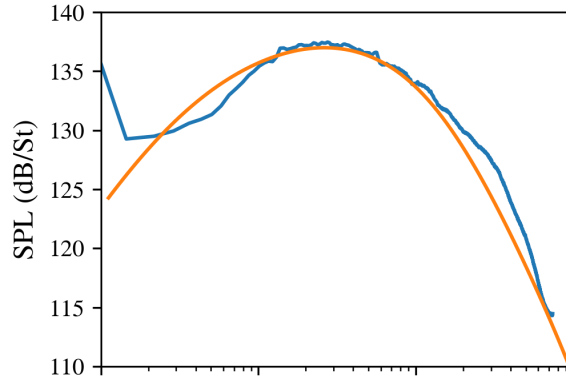


**Fig. 3 Evolution of the characteristic length  $l_s$  along the jet lipline. —, reference computed from the integral length scale of a LES [25], and, —, characteristic length  $l_s$  computed from equation (12) with a proportionality constant of 1.0.**

Having no need to tune the amplitude of the sound source to fit with the measurements is quite satisfactory, this is in agreement with model for the sound source introduced in equation (1), and tends to indicate that the derivations have been successfully completed.

### III. Application to the study of installation effects of a jet under a flat plate

#### A. Studied test case

Two configurations from a test campaign performed in 2014 at the CNRS - Pprime laboratory are investigated in this work. The first is a simple isothermal round jet exhausting a converging nozzle of diameter  $D_j = 0.050$  m with a jet Mach number  $M_j = 0.9$ . The second considers the same jet with identical operating conditions, but installed beneath a rectangular flat plate of chord length  $15D_j$  which spans over  $9D_j$ . The jet is separated from the plate by a distance of  $2D_j$ , so that the aerodynamic interactions of the jet with the plate are negligible. This configuration is in turn particularly well suited to the study of acoustic propagation effects [26] [28] [29]. A photography of the experiment is presented in figure 4.

Measurements are made with an azimuthal array of 18 microphones that can be translated along the jet axis. The array of microphones is circular of diameter  $28.4D_j$ , it can be translated from an axial position  $z \approx -2.5D_j$  to a position  $z \approx 39D_j$ , where the location of the duct exhaust serves as a reference for the  $z$ -axis. The azimuthal angle  $\varphi$  and polar angle  $\theta$  are defined as in figure 4, i.e. the azimuth is null for a microphone set in the plan of the plate.

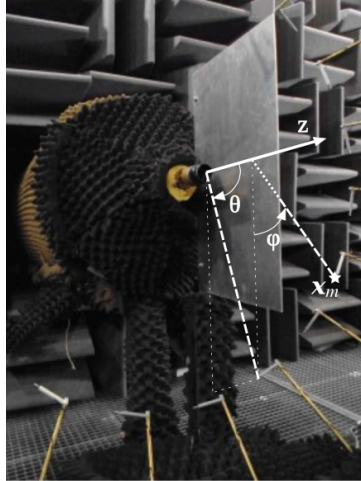


**Fig. 4** Photograph of the mock up under study and definition of the polar and azimuthal angles  $\theta$  and  $\varphi$ .

### B. CFD and CAA analyses

The finite element solver Actran™ is used to compute adjoint Green's functions that are tailored to this configuration. A uniform mesh composed of quadratic elements with tetrahedral shapes is created for the aeroacoustic simulation. Cells are  $0.2D_j$  large and the total mesh possesses  $16 \times 10^6$  DOF. Figure 5 presents the geometry and the mesh considered for the installed jet. The convergent nozzle is modelled within the CAA analysis to mimic at best

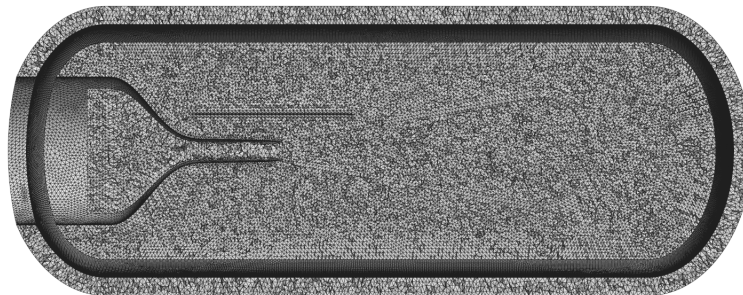


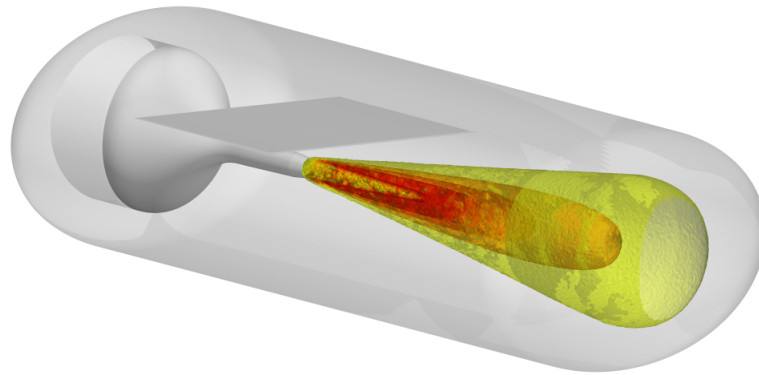
**Fig. 5** Grid used for the aeroacoustic analysis of the installed jet. A uniform mesh with quadratic elements of size  $0.2D_j$  is considered. The transition layer [6] [25] is hidden to better distinguish the different numerical domains.

the experiment. The procedure previously designed with commercial software to compute adjoint Green's functions associated with an observer set out of the computation domain [6] [25] is used anew here. In particular, PML are used to truncate the duct interior volume and to mimic free field propagation outside.

The RANS computations used in this study have been carried out by G. Pont from Airbus Operations using the FLUSEPA 7.2 solver that is based on a  $k-\omega$  turbulence model [30] [28]. Figure 6 displays the evolution of the turbulent kinetic energy  $k$ . No significant interaction of the jet aerodynamic with the flat plate is visible. The CAA grid spans over  $22.5D_j$  downstream of the jet exhaust and is sufficiently large to include all the aeroacoustic sound sources.

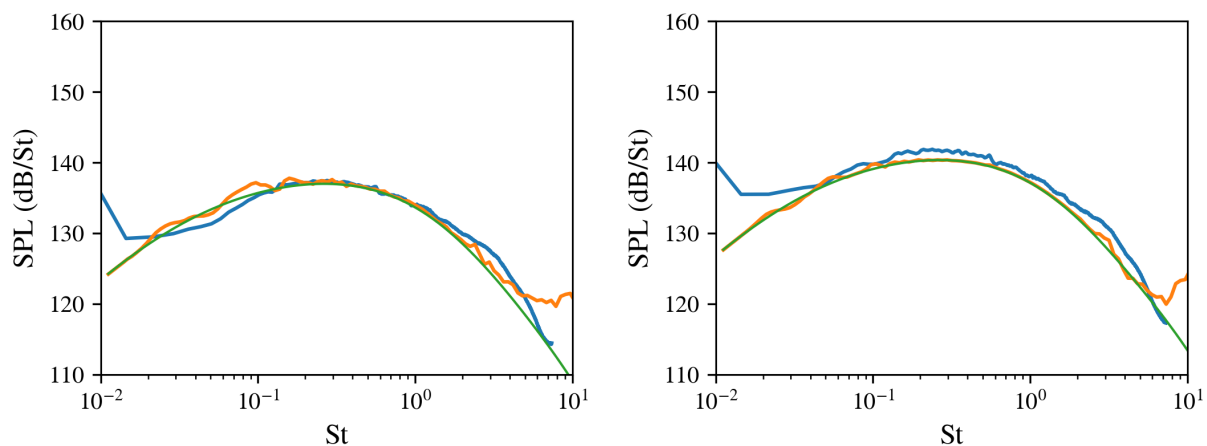
## IV. Acoustic predictions for the isolated jet

The results computed for the isolated configuration are presented first. Tam and Auriault's mixing noise model reformulated for the acoustic potential, and given in equation (9) is used to model the noise emitted by the jet. Noise



**Fig. 6** Isometric view of the CAA domain showing the nozzle geometry and the flat plate. Surfaces of constant turbulent kinetic energy  $k$  are displayed.

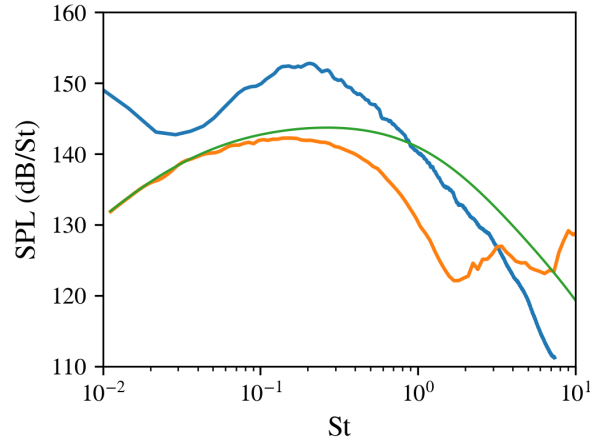
spectra calculated for the polar angle  $\theta = 90^\circ$  and  $\theta = 60^\circ$  are compared to the measurements conducted at the CNRS - Pprime laboratory and presented in figure 7. The predicted acoustic spectra are computed over 100 different Strouhal numbers to logarithmically discretise three decades of Strouhal numbers. All spectra are normalised following equation (14). The predictions at both angles are in close agreement with the measurements in amplitude, shape and



**Fig. 7** Predictions obtained for the polar angles  $\theta = 90^\circ$  (left) and  $\theta = 60^\circ$  (right). —, measurements, —, equation (9) with Actran <sup>TM</sup>'s adjoint Green's functions, and, —, equation (9) with the analytical free field solution given in equation (15).

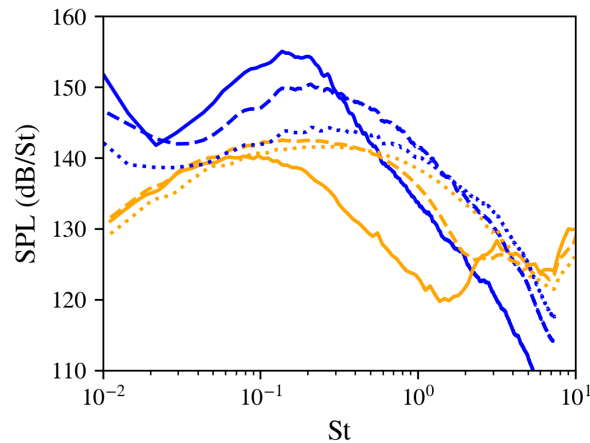
peak position. At  $90^\circ$  the levels between measurements and predictions match remarkably well, at  $60^\circ$  the calculated spectra underpredict the measurements by 1 dB only. For Strouhal numbers greater than 4 the acoustic spectra computed with Actran <sup>TM</sup> becomes incorrect. This is because the CAA grid is too coarse at this frequency to properly describe adjoint Green's functions. Below this limit the prediction computed with Actran <sup>TM</sup> and the one considering simple free field propagation almost coincide.

Figure 8 presents the noise spectra obtained for an observer position forming an angle of  $\theta = 30^\circ$  with the jet axis. The predictions are considerably worse for this shallow angle, and the model misses the measured pic by 10 dB. This time, the predictions computed from the analytical solution fails to capture the correct peak frequency and shape of the acoustic spectra. Shape and peak frequency are noticeably better predicted when using adjoint Green's functions that are tailored to the flow as computed with Actran <sup>TM</sup>. The grid cut-off limit identified previously at a Strouhal number of 4 seems reduced to 1.5. Further effort is required here to better grasp the reason of this unexpected behaviour. This



**Fig. 8** Predictions obtained for  $\theta = 30^\circ$ . —, measurements, —, equation (9) with Actran TM's adjoint Green's functions, and, —, equation (9) with the analytical free field solution given in equation (15).

capacity of the methodology to model the evolution of the noise spectra shape is observed at other shallow polar angles. Figure 9 compares the predictions obtained at  $\theta = 20^\circ$ ,  $\theta = 35^\circ$ , and  $\theta = 50^\circ$  with the corresponding measurements. The continuous deformation of the noise spectra as the observer approaches the jet axis is quite well captured by the model, indicating that refraction effects may be invoked to explain the evolution of the jet noise hump over the polar angles. Figure 10 presents the evolution of the overall sound pressure level (OASPL) computed over the polar angles



**Fig. 9** Predictions at polar angles  $\theta$  shallow to the jet axis. —,  $\theta = 20^\circ$ , ---,  $\theta = 35^\circ$ , and, ·····,  $\theta = 50^\circ$ . —, measurements, and, —, equation (9) with Actran TM's adjoint Green's functions.

$\theta$  for the studied isolated jet. A relatively satisfactory prediction of the levels is obtained with the model proposed for polar angles from  $\theta = 50^\circ$  to  $\theta = 105^\circ$ . Compared to the predictions obtained relying on tailored adjoint Green's functions computed with Actran TM, it is seen that the evolution of the OASPL for observer close to the jet axis is better modelled without taking into account the refraction effects entailed by the jet mean flow, but this is at the cost of a poorer description of the acoustic spectra as illustrated previously. Further work is needed to better capture the level of the sound radiated in the directions shallow to the jet axis [3, fig. 5] [15, fig. 6b]. The better taking into account of the source convection effects or considering a model for the sound radiated by the instability waves are possible areas to improve the present model.

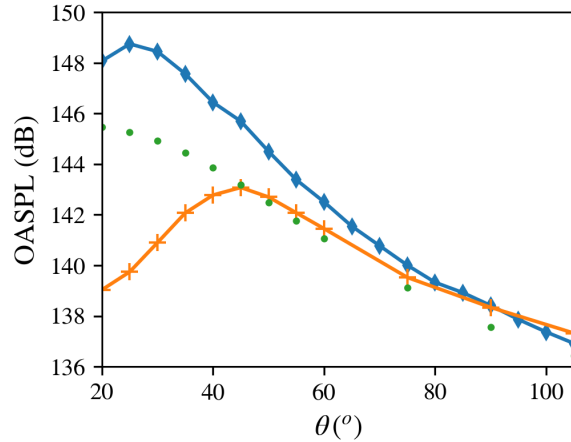


**Fig. 10** Evolution of the OASPL over the polar angles  $\theta$ .  $\blacklozenge$ , measurements,  $+$ , equation (9) with Actran TM's adjoint Green's functions, and,  $\bullet$ , equation (9) with the analytical free field solution given in equation (15).

## V. Acoustic predictions for the installed jet

The noise radiated by the jet installed under the plate is considered here. Only predictions computed in the nozzle exhaust plan are presented. Thus, the polar angle of the observer is set to  $\theta = 90^\circ$  and the evolution over the azimuthal angle  $\varphi$  is investigated. The azimuth is defined as in figure 4. The acoustic predictions obtained in the plan of the plate, that is for  $\varphi = 0^\circ$ , are presented in figure 11. They are compared to the measurements, and to the predictions obtained relying on adjoint Green's functions calculated for the isolated jet configuration. The prediction of the

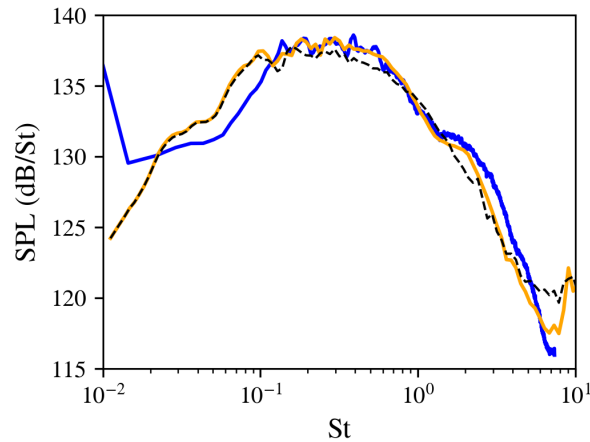


**Fig. 11** Predictions obtained for  $\theta = 90^\circ$  and  $\varphi = 0^\circ$ .  $—$ , measurements, equation (9) with Actran TM's adjoint Green's functions computed,  $—$ , for the installed jet, and,  $- - -$  equation (9), for the isolated jet.

installation effects is well captured by the model, and above a Strouhal number of 0.1 the predicted spectra matches the measurements almost perfectly. Compared to the spectra computed for the isolated jet, the level at the peak frequency increases by 1 dB. A secondary hump for Strouhal numbers within the range 1.5 to 6 is also correctly described.

Predictions computed at azimuthal angles  $\varphi = \pm 20^\circ$  are presented in figure 12. Again, the methodology enables to capture nicely the dynamic of the measured noise spectra. Compared to the predictions relying on Green's functions computed for the isolated jet, the shielding at  $\varphi = 20^\circ$  and the reflection at  $\varphi = -20^\circ$  caused by the plate is correctly described by the model. This reflects for Strouhal numbers greater than 0.6, into a 3 dB attenuation of the noise spectra for  $\varphi = 20^\circ$ , and, into an increase of 3 dB for  $\varphi = -20^\circ$  over the same Strouhal number range.

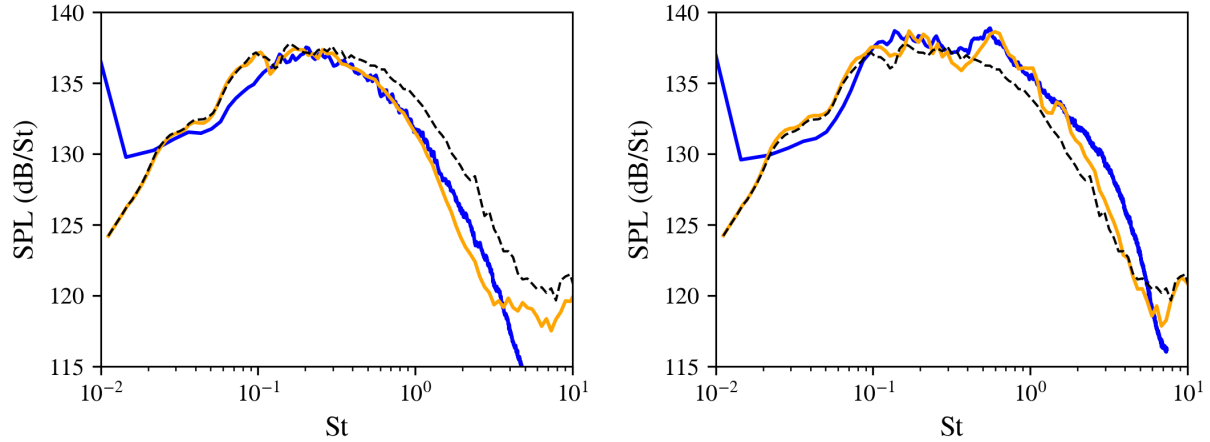


**Fig. 12** Predictions obtained for  $\theta = 90^\circ$  and  $\varphi = 20^\circ$  (left), and, for  $\theta = 90^\circ$  and  $\varphi = -20^\circ$  (right). —, measurements, equation (9) with Actran TM's adjoint Green's functions computed, —, for the installed jet, and, --- equation (9), for the isolated jet.

The azimuthal evolution of the installed jet directivity is presented in figure 13. The OASPL is constant around 140 dB for  $\varphi \leq -20^\circ$ , experiences a transition between  $-20^\circ \leq \varphi \leq 20^\circ$  and reaches plateau about 136 dB for  $\varphi \geq 20^\circ$ . The predicted OASPL agrees with the measured one within 0.5 dB.

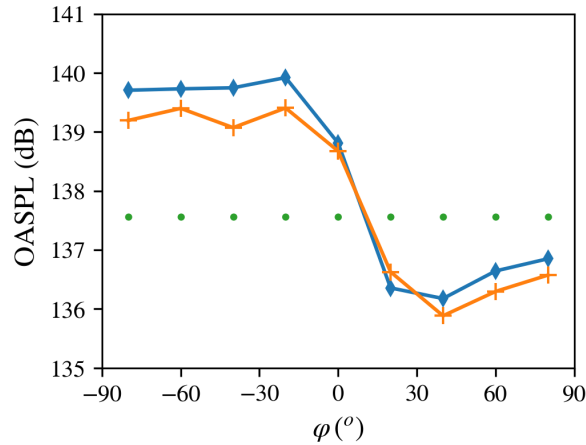


**Fig. 13** Evolution of the OASPL over the azimuthal angles  $\varphi$ . ♦, measurements, +, equation (9) with Actran TM's adjoint Green's functions, and, ●, equation (9) with the analytical free field solution given in equation (15).

## VI. Conclusion

Tam and Auriault's model to predict the sound emitted by the turbulent mixing of a jet is adapted to Pierce's wave equation. A robust formulation is thereby obtained, that enables the use of a numerical solver to calculate the precise propagation of sound. The calibration of the sound source parameters is newly defined, it is solely based on mean flow gradients and the turbulent kinetic energy. The tuning parameters were found unnecessary to obtain very satisfactory results at ninety degree from the jet axis in terms of acoustic level, spectra shape, and central frequency of the jet noise hump. The model gives results within 2 dB of confidence for polar angles greater than  $\theta \geq 50^\circ$ . While initially designed to model the noise from fine scale turbulence, it is found that this reformulation of Tam and Auriault's model does not radiate isotropically. The ability of the methodology proposed to account for propagation effects caused by strong

gradients in the flow and the presence of surfaces is demonstrated. Subtle variations in the acoustic spectra computed for the installed jet configuration could be captured, which paves the way to the aeroacoustic shape optimisation of jet-wing architectures.

### Acknowledgements

The authors are grateful to Grégoire Pont (Airbus Operations) for performing the RANS calculations used in this study, and to Peter Jordan (CNRS - Pprime) for sharing the acoustic spectra measured during the test campaign associated with the investigated configuration. This work was performed within the framework of the AMBROSIA project founded by The French Civil Aviation Authority (DGAC Convention 2019-18), with also the support of the Labex CeLyA of the Université de Lyon, within the programme "Investissements d'Avenir" (ANR-10-LABX-0060/ANR-11-IDEX-0007) operated by the French National Research Agency (ANR).

### References

- [1] Lighthill, M. J., "On sound generated aerodynamically I. General theory," *Proceedings of the Royal Society of London. Series A. Mathematical and Physical Sciences*, Vol. 1107, The Royal Society London, 1952, pp. 564–587.
- [2] Ribner, H. S., "Effects of jet flow on jet noise via an extension to the Lighthill model," *Journal of Fluid Mechanics*, Vol. 321, 1996, pp. 1–24.
- [3] Khavaran, A., "Role of anisotropy in turbulent mixing noise," *AIAA Journal*, Vol. 37, No. 7, 1999, pp. 832–841.
- [4] Morris, P. J., and Boluriaan, S., "The Prediction of Jet Noise from CFD Data," *10th AIAA/CEAS Aeroacoustics Conference*, AIAA Paper 2004-2977, Manchester, 2004. <https://doi.org/10.2514/6.2004-2977>.
- [5] Goldstein, M. E., and Leib, S. J., "The aeroacoustics of slowly diverging supersonic jets," *Journal of Fluid Mechanics*, Vol. 600, 2008, pp. 291–337.
- [6] Spieser, É., Legendre, C., and Bailly, C., "Solution of Pierces equation for Tam & Auriault's mixing noise model," *AIAA Aviation 2021 Forum*, AIAA Paper 2021-2238, Virtual event, 2021, p. 2238. <https://doi.org/10.2514/6.2021-2238>.
- [7] Leib, S. J., and Goldstein, M. E., "Hybrid source model for predicting high-speed jet noise," *AIAA Journal*, Vol. 49, No. 7, 2011, pp. 1324–1335.
- [8] Depuru Mohan, N. K., Dowling, A. P., Karabasov, S. A., Xia, H., Graham, O., Hynes, T. P., and Tucker, P. G., "Acoustic sources and far-field noise of chevron and round jets," *AIAA Journal*, Vol. 53, No. 9, 2015, pp. 2421–2436.
- [9] Ribner, H. S., "Aerodynamic sound from fluid dilations. A theory of the sound from jets and other flows," Tech. rep., University of Toronto, Institute of aerophysics, 1962. UTIA Report N<sup>o</sup> 86, AFOSR TN 3430.
- [10] Tam, C. K. W., and Auriault, L., "Jet mixing noise from fine-scale turbulence," *AIAA Journal*, Vol. 37, No. 2, 1999, pp. 145–153.
- [11] Bailly, C., Lafon, P., and Candel, S. M., "Subsonic and supersonic jet noise predictions from statistical source models," *AIAA Journal*, Vol. 35, No. 11, 1997, pp. 1688–1696.
- [12] Balsa, T. F., "The acoustic field of sources in shear flow with application to jet noise: convective amplification," *Journal of Fluid Mechanics*, Vol. 79, No. 1, 1977, pp. 33–47.
- [13] Khavaran, A., and Bridges, J., "Modelling of fine-scale turbulence mixing noise," *Journal of Sound and Vibration*, Vol. 279, No. 3-5, 2005, pp. 1131–1154. <https://doi.org/10.1016/j.jsv.2003.11.054>, URL <http://linkinghub.elsevier.com/retrieve/pii/S0022460X04000586>.
- [14] Goldstein, M. E., and Rosenbaum, B., "Effect of anisotropic turbulence on aerodynamic noise," *The Journal of the Acoustical Society of America*, Vol. 54, No. 3, 1973, pp. 630–645.
- [15] Afsar, M. Z., Dowling, A. P., and Karabasov, S. A., "Jet noise in the 'zone of silence'," *13th AIAA/CEAS Aeroacoustics Conference*, AIAA Paper 2007-3606, Rome, 2007. <https://doi.org/10.2514/6.2007-3606>.
- [16] Afsar, M. Z., "Insight into the two-source structure of the jet noise spectrum using a generalized shell model of turbulence," *European Journal of Mechanics-B/Fluids*, Vol. 31, 2012, pp. 129–139.

- [17] Balsa, T. F., and Glibe, P. R., "Aerodynamics and noise of coaxial jets," *AIAA Journal*, Vol. 15, No. 11, 1977, pp. 1550–1558.
- [18] Goldstein, M. E., "High frequency sound emission from a moving point multipole sources embedded in arbitrary transversely sheared mean flows," *Journal of Sound and Vibration*, Vol. 80, No. 4, 1982, pp. 499–522.
- [19] Dowling, A. P., Ffowcs Williams, J. E., and Goldstein, M. E., "Sound production in a moving stream," *Philosophical Transactions of the Royal Society A*, Vol. 288, No. 1353, 1978, pp. 321–349.
- [20] Tam, C. K. W., and Auriault, L., "Mean flow refraction effects on sound radiated from localized source in a jet," *Journal of Fluid Mechanics*, Vol. 370, 1998, pp. 149–174.
- [21] Spieser, É., and Bailly, C., "Sound propagation using an adjoint-based method," *Journal of Fluid Mechanics*, Vol. 900, 2020, p. A5. <https://doi.org/10.1017/jfm.2020.469>.
- [22] Ilário, C. R. S., Azarpeyvand, M., Rosa, V., Self, R. H., and Meneghini, J. R., "Prediction of jet mixing noise with Lighthill's Acoustic Analogy and geometrical acoustics," *The Journal of the Acoustical Society of America*, Vol. 141, No. 2, 2017, pp. 1203–1213.
- [23] Martelet, Y., Suratteau, J.-Y., Pont, G., and Bailly, C., "Prediction of Fine-scale Jet Mixing Noise Using Geometrical Acoustics," *25th AIAA/CEAS Aeroacoustics Conference*, AIAA Paper 2019-2755, Delft, 2019. <https://doi.org/10.2514/6.2019-2755>.
- [24] Semiletov, V. A., and Karabasov, S. A., "Adjoint Linearised Euler solver for Goldstein acoustic analogy equations for 3D non-uniform flow sound scattering problems: verification and capability study," *20th AIAA/CEAS Aeroacoustics Conference*, AIAA Paper 2014-2318, Atlanta, Georgia, 2014. <https://doi.org/10.2514/6.2014-2318>.
- [25] Spieser, E., Bogey, C., and Bailly, C., "Noise predictions of a Mach 0.9 round jet using tailored adjoint Greens functions," *Journal of Sound and Vibration*, 2022 – under review.
- [26] Piantanida, S., Jaunet, V., Huber, J., Wolf, W. R., Jordan, P., and Cavalieri, A. V. G., "Scattering of turbulent-jet wavepackets by a swept trailing edge," *The Journal of the Acoustical Society of America*, Vol. 140, No. 6, 2016, pp. 4350–4359.
- [27] Bogey, C., Barré, S., Fleury, V., Bailly, C., and Juvé, D., "Experimental study of the spectral properties of near-field and far-field jet noise," *International Journal of Aeroacoustics*, Vol. 6, No. 2, 2007, pp. 73–92.
- [28] Martelet, Y., "Jet mixing noise model based on geometrical acoustics for the prediction of installation effects," Ph.D. thesis, École Centrale de Lyon, Laboratoire de Mécanique des Fluides et d'Acoustique (LMFA) - CIFRE Airbus Commercial Aircraft, N° 2020LYSEC12, 2020.
- [29] Lyu, B., Dowling, A. P., and Naqavi, I., "Prediction of installed jet noise," *Journal of Fluid Mechanics*, Vol. 811, 2017, pp. 234–268.
- [30] Pont, G., Brenner, P., Cinnella, P., Maugars, B., and Robinet, J. C., "Multiple-correction hybrid k-exact schemes for high-order compressible RANS-LES simulations on fully unstructured grids," *Journal of Computational Physics*, Vol. 350, 2017, pp. 45–83.